# Experimental Implementation of Assisted Quantum Adiabatic Passage in a Single Spin

Jingfu Zhang,[1] Jeong Hyun Shim,[1] Ingo Niemeyer,[1] T. Taniguchi,[2] T. Teraji,[2] H. Abe,[3] S. Onoda,[3] T. Yamamoto,[3] T. Ohshima,[3] J. Isoya,[4] and Dieter Suter[1]

[1]*Fakultät Physik, Technische Universität Dortmund, D-44221 Dortmund, Germany*
[2]*National Institute for Materials Science, 1-1 Namiki, Tsukuba, Ibaraki 305-0044, Japan*
[3]*Japan Atomic Energy Agency, 1233 Watanuki, Takasaki, Gunma 370-1292, Japan*
[4]*Research Center for Knowledge Communities, University of Tsukuba, Tsukuba 305-8550, Japan*
(Received 4 December 2012; revised manuscript received 4 April 2013; published 11 June 2013)

Quantum adiabatic passages can be greatly accelerated by a suitable control field, called a counter-diabatic field, which varies during the scan through resonance. Here, we implement this technique on the electron spin of a single nitrogen-vacancy center in diamond. We demonstrate two versions of this scheme. The first follows closely the procedure originally proposed by Demirplak and Rice [J. Phys. Chem. A **107**, 9937 (2003)]. In the second scheme, we use a control field whose amplitude is constant but whose phase varies with time. This version, which we call the rapid-scan approach, allows an even faster passage through resonance and therefore makes it applicable also for systems with shorter decoherence times.

DOI: 10.1103/PhysRevLett.110.240501 PACS numbers: 03.67.Lx

*Introduction.*—Controlling quantum systems with high fidelity is an essential prerequisite in various fields, such as coherent control of atomic and molecular systems [1] and quantum information processing [2,3]. The strategies that have been developed for this purpose include the adiabatic passage technique, which leads the quantum system along a specific pathway in such a way that the system always remains in its ground state. One of the attractive properties of this technique is that the resulting evolution is robust with respect to some experimental imperfections [4]. The adiabatic passage also is the central part of the adiabatic model of quantum computation [5,6], which has been shown to be equivalent to the more common network model. In all these cases, it is essential that the scan duration of the adiabatic passage is short and the fidelity as high as possible.

The quantum adiabatic theorem guarantees that the system remains approximately in its ground state if the evolution is sufficiently slow [7–9]. However, for all practical applications, the optimal implementation is reached when the scan time remains short, e.g., compared to the decoherence time. A variety of techniques have been developed, such as exploiting nonlinear level-crossing models [10] and amplitude-modulated and composite pulses [11,12].

In a recent development [13–15], it was shown that the system can remain exactly in its ground state, without undergoing transitions, if an additional control field, the so-called the counter-diabatic (CD) field is introduced. This strategy was recently implemented in an atomic Bose-Einstein condensate [16].

In multilevel systems, stimulated Raman transitions can be driven in such a way that populations are transferred adiabatically between two states [17,18]. Adiabatic transfers have also been extended to nonlinear systems, where the theoretical analysis becomes significantly more complicated [19,20].

In this Letter, we report another experimental implementation of the assisted adiabatic passage (AAP), using a single nitrogen-vacancy (NV) center in diamond [21–23]. The NV centers are point defects, each of which consists of a substitutional nitrogen adjacent to a vacancy. The NV centers can exhibit attractive quantum properties even at room temperature [24–26]. The potential applications of the NV centers include quantum metrology [27–30] and quantum computing [31–34]. Various techniques for implementing high-fidelity coherent control of the NV centers have been developed recently [26,29,35,36]. In our experiment, we implement the AAP on an electron spin transition of the NV center, using resonant microwave fields as controls. In contrast to the previous implementation [16], where the coherent control was applied to an ensemble of atoms, our experiment is implemented on a single spin, with a potential advantage in encoding quantum information into qubits in building quantum computers. The fidelity of the passage is sufficiently high that we can perform multiple rounds of the passage in opposite directions. The results show good agreement between theory and experiment.

*Model.*—In close analogy to the Landau-Zener model [37–39], we describe the AAP with the Hamiltonian

$$H_{\mathrm{LZ}}(t) = \lambda(t) I_z + \Delta I_x, \tag{1}$$

where the $I_{x,z}$ are spin operators, and $\lambda(t)$ and $\Delta$ are dimensionless fields applied along the $z$ and $x$ directions. This Hamiltonian is a model for an arbitrary two level system and plays a prominent role in various fields of physics, such as in coherent control [16,40], quantum criticality [41–43], and even in many-body systems [44]. The energy eigenvalues are $\pm\sqrt{\lambda^2(t) + \Delta^2}/2$, and the instantaneous ground state is

 

$$|g(t)\rangle = \sin[\theta(t)/2]|0\rangle - \cos[\theta(t)/2]|1\rangle, \quad (2)$$

where $\tan\theta(t) = \Delta/\lambda$, $\theta \in [0, \pi]$, and $|0\rangle$ and $|1\rangle$ denote the eigenstates of $I_z$ with eigenvalues $\pm 1/2$, respectively. The minimal gap between the two levels is $\Delta$. Figure 1(a) illustrates the energy levels for $\Delta = 0.2$.

The original assisted adiabatic passage model [13,43] starts from a scan from $-\infty$ to $+\infty$. For the experimental implementation, we have to restrict ourselves to a finite range, which we write as $[-b, b]$. If the control field is scanned linearly in time from $-b$ to $b$,

$$\lambda(t) = b(t - 1), \quad (3)$$

where $t \in [0, 2]$. The scheme can then be implemented for any nonzero value of $\Delta$ by introducing a CD field that is perpendicular to both the $x$ and $z$ components of the field:

$$H_{\mathrm{CD}}(t) = V_{\mathrm{CD}}(t) I_y, \quad (4)$$

where

$$V_{\mathrm{CD}}(t) = -(d\lambda/dt)\Delta/[\Delta^2 + \lambda(t)^2], \quad (5)$$

where the rate of change of $\lambda(t)$ is $d\lambda/dt = b$ for the field of Eq. (3). The total field for the AAP is thus a vector $\vec{B}(t) = [\Delta, V_{\mathrm{CD}}(t), \lambda(t)]$. Figure 1(b) shows the time dependence of the three components for $b = 2$.

*Experimental protocols and results.*—For the experimental test, we used the electron spin of a single NV center in $^{12}$C enriched diamond. The reduced number of $^{13}$C nuclear spins results in long relaxation times, with $T_2^* > 100\ \mu$s.

The hyperfine coupling between the electron and the $^{14}$N nuclear spin is $\approx 2.1$ MHz; see the spectrum shown in Fig. 1(a) in the Supplemental Material [45]. For the present experiments, we use the subspace of this system that is spanned by the states $m_S = 0, +1$ of the electron spin, $m_I = 0$ of the nuclear spin. This subsystem can be excited with excellent selectivity if the amplitude of the microwave field remains well below the hyperfine coupling constant. We therefore will not consider the nuclear spin state in the following; see the spectrum shown in Fig. 1(b) in the Supplemental Material [45].

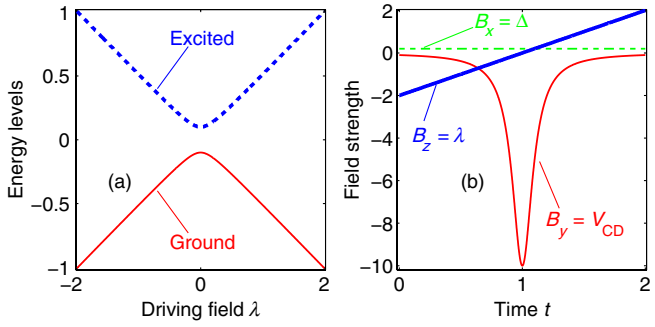


FIG. 1 (color online). Characteristics of the single qubit model for $\Delta = 0.2$ and $b = 2$. (a) the energy levels and (b) the time dependence of the three field components.

For the AAP, the system should be initialized into the ground state $|g(0)\rangle$ of $H_{\mathrm{LZ}}(0)$. In the experiment, we initialize the system by a laser pulse into the state $|0\rangle$, whose overlap with $|g(0)\rangle$ is $\sin[\theta(0)/2]$. In the experiment, we use $-3 \geq \lambda(0)/\Delta \geq -20$, which results in overlaps of $[0.9871, 0.9997]$. For our purpose, this is sufficiently close to unity.

After initialization, the system evolves under the time-dependent Hamiltonian

$$H(t) = H_{\mathrm{LZ}}(t) + H_{\mathrm{CD}}(t) \quad (6)$$

into the state

$$|\psi(t)\rangle = \tilde{U}(t)|g(0)\rangle, \quad (7)$$

where $\tilde{U}(t)$ represents the propagator generated by $H(t)$. During and after the scan, we read out the state of the system by a second laser pulse, which again projects the system onto the state $|0\rangle$. We write the probability of finding the system in this state as $P_{|0\rangle} = |\langle 0|\psi(t)\rangle|^2$. The detailed description of the system and the experiment setup is given in the Supplemental Material [45].

In the actual experiment, the fields $\Delta$, $V_{\mathrm{CD}}$, and $\lambda$ act on the spin in a rotating reference frame. Writing

$$U_r = e^{-i\xi(t)I_z}$$

for the transformation from the laboratory frame to the rotating frame, the Hamiltonians of the two frames are related as

$$\begin{aligned} H^{\mathrm{rot}} &= U_r H^{\mathrm{lab}} U_r^\dagger + i\dot{U}_r U_r^\dagger, \\ H^{\mathrm{lab}} &= U_r^\dagger H^{\mathrm{rot}} U_r - i U_r^\dagger \dot{U}_r. \end{aligned} \quad (8)$$

The laboratory-frame Hamiltonian thus has the field components

$$\begin{aligned} \omega_x(t) &= \Delta\cos\xi(t) + V_{\mathrm{CD}}(t)\sin\xi(t) \\ \omega_y(t) &= -\Delta\sin\xi(t) + V_{\mathrm{CD}}(t)\cos\xi(t) \\ \omega_z &= \lambda(t) - [d\xi(t)/dt]. \end{aligned}$$

This Hamiltonian must match the experimentally available Hamiltonian, whose general form is

$$H^{\mathrm{exp}} = -\omega_0 I_z + 2\omega_1(t) I_x.$$

Accordingly, we must have

$$\xi(t) = \omega_0 t + \int_0^t \lambda(t')dt',$$

which defines our rotating frame transformation. For the transverse field components, we invoke the rotating field approximation, which allows us to set

$$\omega_1(t) = \Delta\cos\xi(t) + V_{\mathrm{CD}}(t)\sin\xi(t)$$

and ignore the $y$ component. The amplitude of the field is therefore

$$|\omega_1(t)| = \sqrt{\Delta^2 + V_{\mathrm{CD}}(t)^2}.$$

Experimental limitations define a maximum possible field amplitude, which we designate as $\Omega$. In the present experiment, it is determined by the requirement that no transitions of other nuclear spin states are excited, and we found a value of $\Omega \approx 2\pi \times 0.2$ MHz to be a suitable compromise. The maximum field amplitude is reached at

$$\Omega = \sqrt{\Delta^2 + [b^2/\Delta^2]}/s_a, \tag{9}$$

where we have defined the scale factor $s_a$, which converts the dimensionless quantities $\Delta$ and $b$ into actual field amplitudes (in Hz) and defines the scan duration

$$\tau_s = 2s_a. \tag{10}$$

Figure 2 shows the experimental results of the AAP for the scan rates $b = 0.6$, 1, 1.6, 2, 3, and 4. For these parameters, we can approximate $s_a \approx b/(\Omega\Delta)$. For $b = 0.6$, the scan duration becomes 4.77 $\mu$s and for $b = 4$ it is 31.83 $\mu$s. The $z$ component is always scanned from $-40$ to $+40$ kHz (in frequency units), while the $y$ component (the CD field) reaches a maximal amplitude of 200 kHz at the anticrossing point. The $x$ component of the field in the rotating frame is 13.3 kHz for $b = 0.6$ and 2.0 kHz for $b = 4$. Filled circles show the experimentally measured probabilities of the state $|0\rangle$. The error bars (1 standard deviation) were determined by repeating each experiment 10 times. The solid lines, which agree very well with the experimental data points, represent the theoretical behavior. For comparison, we also show one data set that was obtained without a CD field, for a scan rate of $b = 2$. These data points are represented by the empty circles and the corresponding theoretical curve can be approximated as a horizontal line going through the experimental points. Clearly, a passage without a CD field results in an almost completely diabatic transfer.

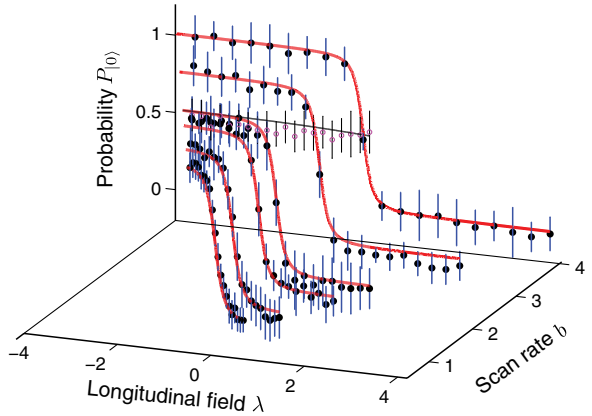


FIG. 2 (color online). Experimental results obtained with the analog implementation of the AAP. The individual experiments correspond to $b = 0.6$, 1, 1.6, 2, 3, and 4. The experimental data are shown as filled circles, and the corresponding error bars were obtained by repeating the experiment 10 times. The curves show the theoretical result for an ideal scan. The empty circles with the almost horizontal line show the result for a reference experiment without a CD field. The 2D representation is shown in the Supplemental Material [45].

Heisenberg's uncertainty relation limits the speed of every (adiabatic or not) state-to-state transfer for a given field strength. It is thus possible to increase the speed by using higher field strengths. On the other hand, the maximum field strength is limited by the properties of the system as well as by experimental limitations. Within these experimental limitations, we now look for a scheme that remains close to the original proposal, but minimizes the overall duration of the scan without exceeding a field strength that is dictated by the experimental conditions. In the following, we will refer to this approach as the rapid scan.

We determine the required control fields by dividing the overall evolution $\tilde{U}(t)$ into $N$ segments [46,47], each of duration $\delta$, with the total duration of the sequence $N\delta = 2$. The evolution within each segment is $U_m = \mathcal{T}\exp[-i\int_{(m-1)\delta}^{m\delta} H(t)dt] \approx \exp[-i\delta H(m\delta)]$, where $\mathcal{T}$ denotes the Dyson time ordering operator. Each segment $U_m$ was implemented as a rectangular pulse with Hamiltonian $H_m = H(m\delta)/s_m$, whose field amplitude had the constant value $\Omega$. $s_m$ is the scaling factor for the segment. The duration of the segment can therefore be reduced by this factor, compared to $\delta$, to $\tau_m = s_m\delta$. Clearly, the reduction of the duration is only limited by the available field strength.

Using the transformation Eq. (8), we can calculate the required laboratory-frame Hamiltonian

$$H_m^{\mathrm{lab}} = -\omega_0 I_z + 2\Omega I_x \cos(\omega_m t + \phi_m)$$

and the required duration $\tau_m$, where $t \in [\sum_{j=1}^{m-1}\tau_j, \sum_{j=1}^{m}\tau_j]$. The scaling factor

$$s_m = \tau_m/\delta = \sqrt{\Delta^2 + V_{\mathrm{CD}}^2(m\delta)}/\Omega \tag{11}$$

is now different for every segment. The angular frequency $\omega_m$ and the phase $\phi_m$ become

$$\omega_m = \omega_0 + [\lambda(m\delta)/s_m], \qquad \tan\phi_m = -V_{\mathrm{CD}}(m\delta)/\Delta.$$

In the Supplemental Material [45], we show the explicit values of these parameters for each step.

Figure 3 shows the experimental results. Here, we used the same nominal scan rates $b$ as in the analog case, but split the scan into $N = 56$ segments. The experimental data points are represented by filled circles, the error bars were obtained by repeating the experiments eight times. Clearly, the experimental data agree very well with the theoretical expectation shown as the red curves. The empty

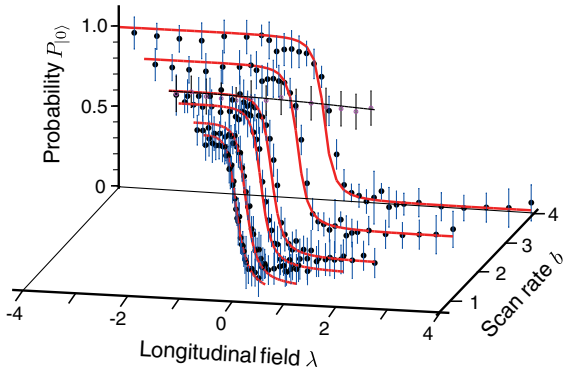


FIG. 3 (color online). Experimental results obtained with the rapid-scan approach. For details see the caption of Fig. 2. The 2D representation is shown in the Supplemental Material [45].

circles again represent the reference experiment obtained by setting $V_{CD} = 0$.

Given the high fidelity obtained in a single passage through resonance, we can cycle the system back and forth multiple times. The reverse passage is obtained by changing $b$ to $-b$, which changes the direction of the scan as well as the sign of the CD field. The results obtained in the analog and rapid-scan approaches are shown as the left and right columns in Fig. 4. Figures 4(a) and 4(c) show the three field components in the rotating frame, and Figs. 4(b) and 4(d) represent the experimental results for these repetitive scans, as well as the theoretical curves corresponding to the ideal case. We find very little loss of population after five passages through resonance.

*Discussion.*—The experimental implementation of the time-dependent Hamiltonian $H(t)$ always occurs with finite precision, which results in a loss of fidelity. Experimental contributions to this loss include the precision with which the shaped pulses are implemented—both in terms of the amplitude and in terms of the time

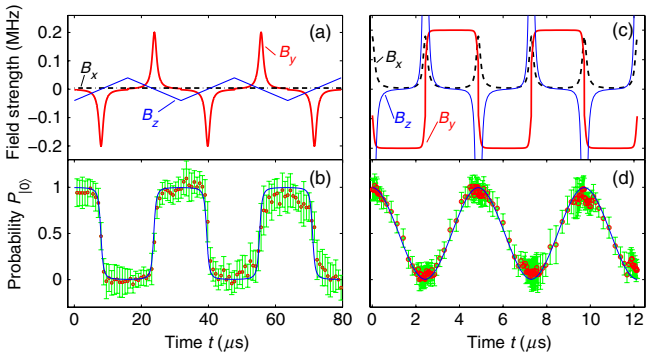


FIG. 4 (color online). Multiple assisted adiabatic passages. The results obtained in the analog and rapid-scan approaches are shown in the left and right columns, respectively. (a) and (c) show the three components of the applied fields, while (b) and (d) show the experimental data, together with the theoretical curves for the ideal case (zero loss).

resolution. In the rapid-scan approach, the number of segments used is an important parameter. We used numerical simulations of the experiment to estimate these losses. The results indicate that for the analog scan, finite time resolution of 0.25 ns reduces the fidelity by a fraction of the order of $10^{-8}$. In the rapid-scan approach, for $N = 56$ segments, the maximal loss during the AAP occurs near the critical point at $\lambda = 0$. For the lowest scan rate, with $b = 0.6$, this loss is of the order of $<10^{-3}$, for the faster scan rate, $b = 4.0$, it rises to $2.8 \times 10^{-2}$. However, these are mostly intermediate losses, which are recovered during the second part of the scan: The calculated loss of fidelity at the end of the evolution period is $<10^{-4}$.

For the parameters chosen here, the duration of a single scan varies between 4.77 and 31.83 $\mu$s in the analog version and from 2.0 to 2.5 $\mu$s in the rapid-scan implementations. They are thus all short compared to the coherence time of our sample ($T_2 \approx 500$ $\mu$s).

To estimate the speed-up provided by the CD field, we used numerical simulations of an unassisted scan, with the same parameters as the experimental scan in Fig. 2, but slower scan rates. To reach a fidelity of 0.99, the scan duration had to be extended to 2.33 ms. This implies that the assisted scan allows a speed-up of more than 2 orders of magnitude ($\sim 150$) if a linear frequency scan is used and of about 3 orders of magnitude ($\sim 960$) in the rapid passage (constant amplitude) version.

The analog and the rapid-scan approaches implement both the same propagator, but they use a different scaling of the time axis. This allows one to scan very rapidly when the quantization axis does not change appreciably with the offset. Most of the speed advantage of the rapid-scan approach is therefore gained in the region of large detunings (see Fig. 3 in the Supplemental Material [45]). Both experiments relied on a segmentation of the actual fields for implementation in an arbitrary waveform generator. The precision with which the scans can be implemented depend therefore on the amplitude and time resolution of the instrument. In our setup, the minimal possible time resolution is 0.25 ns, which is significantly shorter than the time step used here ($> 6.4$ ns). According to numerical simulations, using the full time resolution would reduce the loss of fidelity due to the segmentation to $<10^{-7}$. The rapid-scan approach presented here is a first attempt at reducing the duration of an AAP scan. We are confident that further improvements are possible, e.g., by using the tools of optimal control theory.

*Conclusion.*—We have implemented the assisted adiabatic passages through analog and rapid-scan approaches in a two level quantum system by controlling a single spin in a NV center in diamond. This approach allows a significant increase in the scan rate compared to the unassisted passage and therefore reduces the requirements on the decoherence time of the system to which it is applied. Like in the unassisted case, the scan has to be slower if

the minimum gap is small. If the scan is performed linearly in time, the total duration also increases with the scan range. However, with the rapid-scan approach that we introduced here, the scan range can be increased arbitrarily with very little time penalty. Our experiment results illustrate the excellent coherent control that can be achieved for the spins of NV centers. These results should be helpful for all applications requiring quantum adiabatic passages, such as implementing geometric gates for quantum computation [48], adiabatic control in interacting two level systems [49], or adiabatic quantum computing [6].

This work is supported by the Heinrich Hertz Foundation, and the DFG through grant Su 192/27-1.

[1] P. Král, I. Thanopulos, and M. Shapiro, Rev. Mod. Phys. **79**, 53 (2007).
[2] M. Nielsen and I. Chuang, *Quantum Computation and Quantum Information* (Cambridge University Press, Cambridge, England, 2000).
[3] J. Stolze and D. Suter, *Quantum Computing: A Short Course from Theory to Experiment* (Wiley-VCH, Berlin, 2008), 2nd ed.
[4] A. M. Childs, E. Farhi, and J. Preskill, Phys. Rev. A **65**, 012322 (2001).
[5] E. Farhi, J. Goldstone, S. Gutmann, and M. Sipser, arXiv: quant-ph/0001106v1.
[6] E. Farhi, J. Goldstone, S. Gutmann, J. Lapan, A. Lundgren, and D. Preda, Science **292**, 472 (2001).
[7] J. Du, L. Hu, Y. Wang, J. Wu, M. Zhao, and D. Suter, Phys. Rev. Lett. **101**, 060403 (2008).
[8] D. M. Tong, K. Singh, and L. C. Kwek, and C. H. Oh, Phys. Rev. Lett. **95**, 110407 (2005).
[9] K.-P. Marzlin and B. C. Sanders, Phys. Rev. Lett. **93**, 160408 (2004).
[10] N. V. Vitanov and K.-A. Suominen, Phys. Rev. A **59**, 4580 (1999)
[11] N. V. Vitanov, L. P. Yatsenko, and K. Bergmann, Phys. Rev. A **68**, 043401 (2003).
[12] B. T. Torosov, S. Guérin, and N. V. Vitanov, Phys. Rev. Lett. **106**, 233001 (2011).
[13] M. Demirplak and S. A. Rice, J. Phys. Chem. A **107**, 9937 (2003).
[14] M. V. Berry, J. Phys. A **42**, 365303 (2009).
[15] X. Chen, I. Lizuain, A. Ruschhaupt, D. Guéry-Odelin, and J. G. Muga, Phys. Rev. Lett. **105**, 123003 (2010).
[16] M. G. Bason, M. Viteau, N. Malossi, P. Huillery, E. Arimondo, D. Ciampini, R. Fazio, V. Giovannetti, R. Mannella, and O. Morsch, Nat. Phys. **8**, 147 (2012).
[17] K. Bergmann, H. Theuer, and B. W. Shore, Rev. Mod. Phys. **70**, 1003 (1998).
[18] N. V. Vitanov, T. Halfmann, B. W. Shore, and K. Bergmann, Annu. Rev. Phys. Chem. **52**, 763 (2001).
[19] H. Pu, P. Maenner, W. Zhang, and H. Y. Ling, Phys. Rev. Lett. **98**, 050406 (2007).
[20] A. P. Itin and S. Watanabe, Phys. Rev. Lett. **99**, 223903 (2007).
[21] J. H. N. Loubser and J. A. Wyk, Rep. Prog. Phys. **41**, 1201 (1978).
[22] M. W. Doherty, N. B. Manson, P. Delaney, and L. C. L. Hollenberg, New J. Phys. **13**, 025019 (2011).
[23] M. W. Doherty, F. Dolde, H. Fedder, F. Jelezko, J. Wrachtrup, N. B. Manson, and L. C. L. Hollenberg, Phys. Rev. B **85**, 205203 (2012).
[24] T. Gaebel *et al.*, Nat. Phys. **2**, 408 (2006).
[25] P. Neumann *et al.*, Nat. Phys. **6**, 249 (2010).
[26] T. van der Sar, Z. H. Wang, M. S. Blok, H. Bernien, T. H. Taminiau, D. M. Toyli, D. A. Lidar, D. D. Awschalom, R. Hanson, and V. V. Dobrovitski, Nature (London) **484**, 82 (2012).
[27] J. R. Maze *et al.*, Nature (London) **455**, 644 (2008).
[28] G. Balasubramanian *et al.*, Nature (London) **455**, 648 (2008).
[29] N. Zhao *et al.*, Nat. Nanotechnol. **7**, 657 (2012).
[30] M. Loretz, T. Rosskopf, and C. L. Degen, Phys. Rev. Lett. **110**, 017602 (2013).
[31] F. Jelezko and J. Wrachtrup, Phys. Status Solidi (a) **203**, 3207 (2006).
[32] J. Wrachtrup and F. Jelezko, J. Phys. Condens. Matter **18**, S807 (2006).
[33] T. D. Ladd, F. Jelezko, R. Laflamme, Y. Nakamura, C. Monroe, and J. L. O'Brien, Nature (London) **464**, 45 (2010).
[34] D. DiVincenzo, Nat. Mater. **9**, 468 (2010).
[35] A. Gruber, A. Dräbenstedt, C. Tietz, L. Fleury, J. Wrachtrup, and C. von Borczyskowski, Science **276**, 2012 (1997).
[36] X. Xu *et al.*, Phys. Rev. Lett. **109**, 070502 (2012).
[37] L. D. Landau and E. M. Lifshitz, *Quantum Mechanics* (Pergamon, London, 1958).
[38] C. Zener, Proc. R. Soc. A **137**, 696 (1932).
[39] S. N. Shevchenko, S. Ashhab, and F. Nori, Phys. Rep. **492**, 1 (2010).
[40] E. Barnes and S. Das Sarma, Phys. Rev. Lett. **109**, 060401 (2012).
[41] B. Damski, Phys. Rev. Lett. **95**, 035701 (2005).
[42] F. M. Cucchietti, J.-F. Zhang, F. C. Lombardo, P. I. Villar, and R. Laflamme, Phys. Rev. Lett. **105**, 240406 (2010).
[43] A. del Campo, M. M. Rams, and W. H. Zurek, Phys. Rev. Lett. **109**, 115703 (2012).
[44] D. A. Garanin and R. Schilling, Phys. Rev. B **71**, 184414 (2005).
[45] See the Supplemental Material at http://link.aps.org/supplemental/10.1103/PhysRevLett.110.240501 for additional details on (1) The NV center and the experimental setup; (2) Two-dimensional representation of the experimental results and (3) Numerical simulations for optimizing the driving field.
[46] R. Somma, G. Ortiz, J. E. Gubernatis, E. Knill, and R. Laflamme, Phys. Rev. A **65**, 042323 (2002).
[47] X. Peng, J. Du, and D. Suter, Phys. Rev. A **71**, 012307 (2005).
[48] H. Wu *et al.*, Phys. Rev. A **87**, 032326 (2013).
[49] R. T. Brierley, C. Creatore, P. B. Littlewood, and P. R. Eastham, Phys. Rev. Lett. **109**, 043002 (2012).